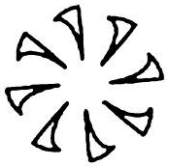

Proceedings of the 15th International Symposium on Unsteady Aerodynamics, Aeroacoustics & Aeroelasticity of Turbomachines
ISUAAAT15
24-27 September 2018, University of Oxford, UK

ISUAAAT15-061

FULLY COUPLED AEROELASTIC SIMULATIONS OF LIMIT CYCLE OSCILLATIONS IN THE TIME DOMAIN

Christian Berthold*
Institute of Propulsion Technology
German Aerospace Center (DLR)
Cologne, Germany

Guido Dhondt
MTU Aero Engines AG
Munich, Germany

Christian Frey
Institute of Propulsion Technology
German Aerospace Center (DLR)
Cologne, Germany

Harald Schönenborn
MTU Aero Engines AG
Munich, Germany

ABSTRACT

In this study a fully coupled aeroelasticity simulation in the time domain of a low pressure turbine (LPT) is demonstrated. The transformation from the unloaded blade geometry to the loaded (consisting of the steady pressure and centrifugal forces) geometry is considered in the initialisation of the coupled solver. The fluid-structure interaction (FSI) solver consists of the flow solver TRACE and the structural solver CalculiX. After validation of the FSI solver its performance and behavior is evaluated in terms of simulation time and capabilities for limit cycle oscillations.

INTRODUCTION

Turbomachinery components are exposed to unsteady aerodynamic loads which must be considered during the design process to ensure the structural mechanical integrity. There are two primary mechanisms which cause structural vibrations and can lead to high-cycle fatigue due to high dynamic stresses: flutter (self-excited vibrations) and forced response (forced excitation, e.g. wakes from upstream blade rows). In industry linear methods are preferred to evaluate aerodynamic designs with respect to vibrations [1,2] while on the structural side nonlinear frequency domain methods are commonly used [3]. This process often imposes conservative limitations on the design space. To further improve the efficiency of turbomachinery components it is necessary to increase the acceptable design space. Thus more accurate analysis methods are needed to evaluate designs and still guarantee a safe operation. Moreover the evaluation of nonlinear effects in the flow and structure are of increasing interest [4] and not all physical causes of vibrations can be modeled with frequency domain methods [5]. Time accurate FSI solvers provide such functionality, although such simulations can be very expensive.

The aim of this paper is to propose an approach for a fully coupled aeroelastic simulation for turbomachinery components. The validation procedure of the FSI solver is presented and the coupled simulation method is applied to an LPT testcase for an LCO analysis. Important topics are highlighted and the behaviour of the solver is investigated.

*Address all correspondence to this author.

NOMENCLATURE

i	complex unit
u	FEM nodal displacement vector
v	FEM nodal velocity vector
v	FEM nodal velocity vector
K	FEM stiffness matrix
M	FEM mass matrix
F	FEM external nodal force vector
F_{ae}	FEM nodal aerodynamic force vector
F_{nl}	FEM nodal nonlinear force vector
f	modal force vector
$\tilde{K}$	modal stiffness matrix
$\tilde{M}$	modal mass matrix
y	modal displacement
Ψ	structural eigenmode
q	vector of conservative flow variables
p	pressure
n	surface normal vector
σ	interblade phase angle (IBPA)
ω	angular frequency
T_{bl}	bilinear interpolation matrix
T_{nn}	nearest neighbour interpolation matrix
T_{co}	conservative interpolation matrix
CFD	Computational Fluid Mechanics
CSM	Computational Structure Mechanics
FEM	Finite Element Method
FSI	Fluid-Structure Interaction
FVM	Finite Volume Method
IBPA	Inter Blade Phase Angle
LCO	Limit Cycle Oscillation
LPT	Low Pressure Turbine

TESTCASE

The test case is provided by MTU Aero Engines AG. The Youngs modulus of the blades is decreased such that the blade row is aerodynamically unstable. The blade row has a shroud with joints which introduce nonlinear damping. The dynamics of the structure are approximated with a few eigenmodes and for the eigenmode analysis sliding boundary conditions for the contact surfaces are deployed. The contact model is a simple regularized and nodal coulomb friction model. In Figure 1 the deflections of the first eigenmode with an Interblade Phase Angle (IBPA) of 72° of the LPT blade row are shown. This eigenmode is excited during the coupled simulation and due to its cyclic symmetry only 5 flow passages must be modeled. On the structure side a full blade row is simulated. A total of 50 passages of flow data is constructed by copying and rotating the flow domain 10 times before the surface pressure is passed to the structural solver.

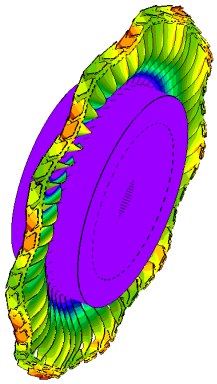

FIGURE 1: LPT blade row with eigenmode deflections.

THEORY AND NUMERICAL METHODS

The flow solver TRACE [6] and the structural solver CalculiX [7] are coupled with a serial approach.

Interpolation of surface data at the fluid-structure interface

To interpolate the surface displacements and velocities from the structural mesh to the fluid mesh bilinear interpolation is used. Therefore the cell faces of the structural mesh surface are divided into sub-triangles. For each vertex of the fluid mesh surface the nearest sub-triangle with a similar surface orientation is identified. Subsequently the displacements and velocities of the structural surface mesh at a fluid mesh vertex are reconstructed by a projection of the vertex onto the sub-triangle plane followed by a bilinear interpolation of displacement data from the corners of the sub-trianlge to the projected vertex of the fluid mesh node. The resulting relation between the displacements u_i^s (or velocity v_i^s) for each spatial direction i of the solid mesh surface and the dispalcements of the fluid mesh surface u_i^f can be expressed as

$$u_i^f = T_{bl} u_i^s \tag{1}$$

For the interpolation of the pressure in the opposite direction nearest neighbour or conservative interpolation is used. In case of the nearest neigbour approach the face centered pressure data of the fluid mesh p^f is interpolated to the faces of the structural mesh surface p^s by determining the nearest fluid face for each structural face (and checking for similar surface orientation) resulting in the transformation rule

$$p^s = T_{nn} p^f . \tag{2}$$

The resulting transformation matrix T_{nn} consists of a single one in each row with the remaining entries being equal to zero re-

sulting in a consistent [8] interpolation of the pressure.

For a conservative interpolation the method presented in [9] is used. To achieve the conservation of performed work at the fluid-structure interface the pressure at the fluid side is converted to discrete vertex based forces by computing the normal force due to the pressure at each mesh vertex:

$$f_i^f = P_i^f p^f \tag{3}$$

for each spatial direction $i = x,y,z$. The discrete forces are interpolated by the transpose of T_{bl} and finally the resulting forces $f_i^s = T_{bl}^T f_i^f$ are projected onto the surface normals of the structural mesh and weighted by the face areas ($p = P_x^s f_x^s + P_y^s f_y^s + P_z^s f_z^s$). The whole interpolation rule can be expressed as

$$p^s = \left(P_x^s T_{bl}^T P_x^f + P_y^s T_{bl}^T P_y^f + P_z^s T_{bl}^T P_z^f\right) p^f = T_{co} p^f \tag{4}$$

Although the discrete forces are mapped in a conservative way, the method presented here introduces small errors due to small local deviations in the surface normal orientation of the adjacent fluid and solid mesh surface. However the implementation of the presented approach requires much less effort than more elaborated methods e.g. [8].

Fluid mechanics modeling

The compressible flow is modeled with the Unsteady Reynolds Averaged Navier-Stokes (URANS) equations. For the closure of the URANS equations the $k-\omega$ turbulence model by Wilcox [10] is used. The intgral form of the URANS equation in Arbitrary Lagrangian-Eulerian form reads

$$\frac{\partial}{\partial t}\int_{V(t)} q_i \, dV + \int_{S(t)} \left(F_{ij} n_j - q_i \frac{dx_j}{dt} n_j\right) dS = 0 \tag{5}$$

with F_{ij} containing all flux vectors as columns. This formulation is appropriate for applications on moving FVM meshes due to the deformation of solid surfaces. For the spatial discretization a second order scheme with a limiter is used and the resulting semi-discrete equations are integrated in time with the BDF2 scheme. To determine the normal face velocity $\frac{dx_j}{dt} n_j$ in order to evaluate the flux term the Discrete Geometric Conservation Law [11] is consistently applied accounting for the BDF2 scheme. 1D nonreflecting boundary conditions [12] are used for the inlet and exit of the fluid domain since these do not require information about the frequency of the flow perturbations which are not known a priori but are part of the solution.

Fluid mesh deformation

To deform the fluid mesh each timestep according to the updated solid deformation a Laplace equation is solved with a GMRES solver for the displacements. Due to the iterative procedure of the GMRES algorithm the mesh deformation from the last timestep is used as initialisation for the next timestep thereby increasing the performance. During development this method performed a few times faster than an explicit inverse distance weighting method with data reduction and parallelisation (see [13]).

Solid mechanics modeling

The discs and blades are discretized by the FEM and the discrete equation of motion reads

$$M\ddot{u} + Ku = F_{ext} \tag{6}$$

with F_{ext} being the external force vector. In a preprocessing procedure the eigenmodes Ψ_i of the disc and blades are determined. Before the eigenmodes are computed static loading (centrifugal forces) is applied to the model. With these loads a static geometrically nonlinear analysis is performed and subsequently the FEM model is linearized around this point. To allow a relative motion between the opposing contact surfaces multiple point constraints are applied to a few points of each surface such that the contact nodes can slide inside the contact plane. In a final step the eigenmodes of the structure are determined by an eigenvalue analysis. On the subspace spanned by the N lowest modeshapes Ψ_i Eq. (6) can be transformed into a reduced model with modal coordinates y:

$$\tilde{M}\ddot{y} + \tilde{K}y = f. \tag{7}$$

The solid mechanics solver has no capability (in modal dynamics and slave mode) to simulate only a few blade sectors given a specific circumferential symmetry and thus the full blade row must be modeled.

In the joints located at the shroud dry friction is modeled with coulomb's law. The contact model between the sliding contact surfaces in the shroud is scetched in Figure 2. A spring and a nonlinear damping element are connecting two FEM nodes (each belonging to one of the contact surfaces). The nonlinear damping element is used to model dry friction and the additional spring element makes the contact situation more realistic. The spring is considered during the eigenmode analysis of the structure and thus is implicitly contained in the modal stiffness matrix $\tilde{K}$. The force of the nonlinear damping element at node i is modeled according to

$$F_{nl,i} = \frac{\Delta\vec{v}_i}{|\Delta\vec{v}_i|} F_n \, \mu \, \phi(\Delta\vec{v}_i) \tag{8}$$

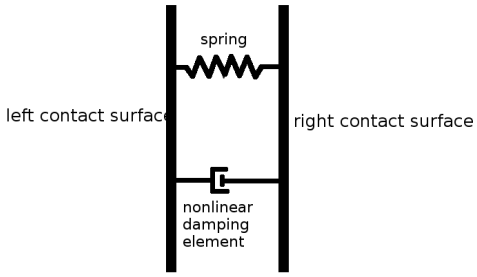

FIGURE 2: Contact friction model.

with

$$\phi(\Delta\vec{v}_i) = \frac{|\Delta\vec{v}_i|^2}{|\Delta\vec{v}_i|^2 + \varepsilon^2}. \tag{9}$$

F_n is the normal force, μ the friction coefficient, ε a friction model coefficient and $\Delta\vec{v} = \vec{v}_i - \vec{v}_{i,\text{opposite}}$ the relative velocity between the two FEM nodes. The modal force vector f in Eq. 7 can then be split and computed according to

$$f = f_{ae} + f_{nl} = \sum_{l=0}^{N} \Psi_l^T F_{ae} + \sum_{l=0}^{N} \Psi_l^T F_{nl} \tag{10}$$

with F_{ae} being the aerodynamic forces and F_{nl} the nonlinear forces containing all $F_{nl,i}$.

Coupling of the two solvers

In this study data between the two surfaces is exchanged at each timestep without further subiteration which is also known as loose coupling. At the beginning of a new timestep the surface pressure is extrapolated with second order extrapolation. Subsequently the structural solver computes the displacements for the next timestep and finally the flow solver computes the new flowfield. The interpolation of surface data is always performed between the two solver executions and the mesh deformation solver is integrated into the flow solver.

Initialization of the unsteady simulation

To initialize the solver a static precalculation of the structure is carried out. Firstly because in a standard industry design process usually the structural FEM mesh is based on the unloaded blade geometry without centrifugal forces and steady pressure. On the other hand the fluid FVM mesh is based on the loaded blade geometry. Thus the static precalculation is done for the structure with the steady pressure loads and centrifugal forces and afterwards the static deformations are stored in order to use these as an offset during the coupled simulation. In the following coupled simulation the offset displacements are subtracted from the displacements coming from the solid dynamics solver before these are passed to the flow solver. Secondly, by computing the static deflections due to the steady loads the structural model is appropriately initialized for the coupled simulation preventing a discontinuous surface pressure jump which would induce a step response of the structure. Here it is assumed that the initial flow field is the steady flow field which is computed in a steady CFD analysis. In a second step after the static analysis an initial motion is introduced to the structure. This enables the excitation of a specific traveling wave motion. In this study an artificial force perturbation distributed around the blade row with a specified IBPA and frequency is used to create the initial motion. The simulation duration for the initial motion is a few periods until the desired initial amplitude for the coupled simulation is obtained. During this time only the structural solver is executed. The artificial force vector direction $\vec{n}_j^{ar}$ for each blade j points in the direction of the axis of symmetry and thus it is not required to transform the vector according to the blade pitch. The artificial force perturbation can then be applied at each timestep t_n:

$$\vec{f}_j^{ar} = A\vec{n}_j^{ar} e^{i(\omega t_n + j\sigma)} \tag{11}$$

with A being the amplitude, ω the angular frequency and σ the IBPA in radians of the perturbation. The steady surface pressure is not removed during this final initialization step.

Evaluation of the modal forces

An important topic for flutter analysis is the evaluation of the modal force if the structural solver is in modal dynamics mode. The modal force f_i with respect to a structural modeshape Ψ_i is defined as

$$f_i = \int_\Gamma \Psi_i^H(x) p(x,t) \vec{n}(x,t) dS(x). \tag{12}$$

For a frequency domain flutter analysis the first order terms of the harmonic pressure and the harmonic surface normal vector variation are retained:

$$\hat{f}_i = \int_\Gamma \Psi_i^H(x) \left(\hat{p}(x)\vec{n}_0(x) + p_0(x)\hat{\vec{n}}(x) \right) dS(x). \tag{13}$$

which will result in a contribution to the aerodynamic damping due to the variation of the surface normals integrated against the mean pressure p_0. Depending on the implementation of the evaluation of the modal force in the time accurate CSM solver the last term in Eq. (13) may not be accounted for. In a linear

spirit the modal force is usually computed according to

$$f_i = \int_\Gamma \Psi_i^H(x)\, p(x,t)\, \vec{n}_0(x)\, dS(x) \tag{14}$$

leading to results which are not consistent with standard flutter analysis tools. To make the time accurate FSI solver yield consistent results the modal forces have to be evaluated according to Eq. (12) with $\vec{n}(x,t)$ depending nonlinearly on the deformed geometry.

APPLICATION

The modal analysis of the full cascade was performed for the first 150 eigenmodes of the structure. For the time accurate simulations the focus is laid on the first mode with an IBPA of $\pm 72^\circ$ which is shown in Figure 1. The in-vacuum eigenfrequency of this mode is 315.03 Hz and consequently the structural motion for all coupled simulations presented in the following are initialized with a force perturbation according to Eq. (11) with $\sigma = \pm\frac{72^\circ}{360^\circ} \cdot 2\pi$ and $\omega = 315.03\text{Hz} \cdot 2\pi$. The $\pm$ sign specifies a forward or backward traveling wave. Due to the cyclic symmetry of the selected IBPA only 5 flow passaged need to be simulated to circumvent the use of phase-lag boundary conditions at periodic boundaries which are not a valid method for in- or decreasing oscillations. Furthermore the simulation of 5 flow passages prevent traveling wave motions with IBPAs other than an integer multiple of $\pm 72^\circ$. To prevent the unstable mode with IBPA$= +144^\circ$ from interfering a small amount of modal damping is added to it. The FVM mesh has 500000 cells and uses wall functions.

The nearest neighbour or conservative method are used for the interpolation of the pressure. Figure 3 shows the steady pressure on the CFD mesh surface as well as the interpolated pressure on the FEM mesh surface with both interpolation methods. The contour of the interpolated pressure using the nearest neighbour method shows minor inaccuracies due to the coarse discretization of the structure. The conservative method suffers from significant overshoots and undershoots at the leading and trailing edges and additionally some spatial oscillations of the interpolated pressure can be observed. Thus for a full FEM time integration scheme conservative interpolation methods could yield unacceptable results due to large unphysical pressure perturbations. In this case however only 150 eigenmodes are used to approximate the motion of the structure which renders the structure unable to respond to perturbations with high spatial wavenumbers such as the pressure perturbations arising from conservative interpolation.

For validation the FSI solver is compared against linear results for an aerodynamically stable as well as an unstable traveling wave mode. For this purpose the nonlinear contact force

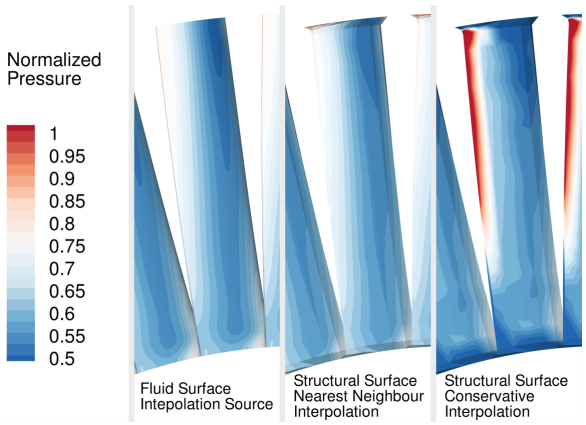

FIGURE 3: Comparison of interpolation methods for the surface pressure mapping.

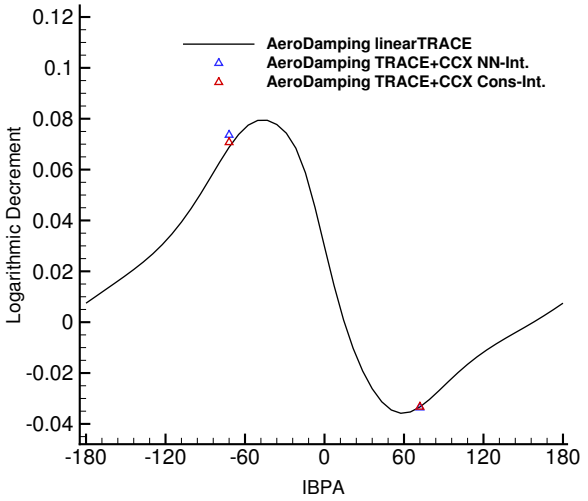

FIGURE 4: Aerodynamic damping over inter-blade phase angle of the LPT blade row.

in the shroud is deactivated. Figure 4 shows a flutter curve of the LPT stage computed with the linearized flow solver linearTRACE. A wide range of IBPAs are aerodynamically unstable. The unstable behaviour for this academic testcase was achieved by decreasing the Youngs's modulus of the blades by a factor of 10 thus decreasing the eigenfrequencies of the structural modeshapes which in turn leads to a low reduced frequency [14].

The data points at the IBPAs $+72^\circ$ (unstable mode, excited) and -72° (stable mode, damped) are computed with the coupled FSI solver for both pressure interpolation methods and 64 timesteps per period. Very good agreement can be observed for IBPA $= +72^\circ$. The aerodynamic damping val-

IBPA $+72^\circ$	linearTRACE	TRACE+CCX (NN)	TRACE+CCX (Cons.)
Log. dec.	-3.335%	-3.361%	-3.330%
Frequency	315.02 Hz	314.89 Hz	315.10 Hz

IBPA -72°	linearTRACE	TRACE+CCX (NN)	TRACE+CCX (Cons.)
Log. dec.	6.879%	7.366%	7.069%
Frequency	315.58 Hz	313.16 Hz	315.36 Hz

TABLE 1: LPT bladerow: linear flutter results.

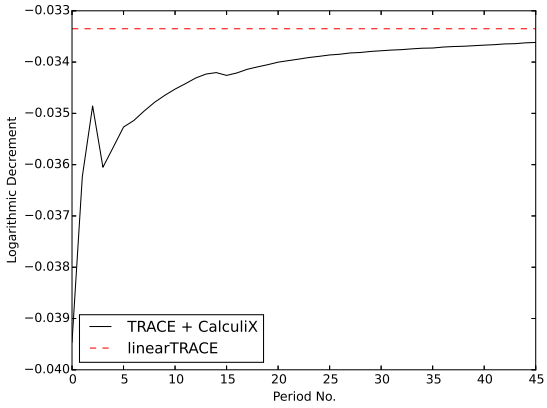

FIGURE 5: Logarithmic decrement per period of the excitet mode (IBPA $= +72^\circ$).

ues for IBPA -72° deviate from the linear results because the logartihmic decrement must be evaluated after a a few periods and the oscillating motion is not perfectly converged. This is necessary since with continuing time the unstable mode (IBPA $+72^\circ$) starts to vibrate and the two modes cannot be distinguished anymore. In Table 1 numerical data of the above results is listed. All values agree well except with the above mentioned shortcoming. Especially the damping values and vibration frequencies computed with the conservative interpolation approach agree best with the linear results. The transient logarithmic decrement and displacement in the shroud are plotted in Figures 5 and 6. It can be observed that the logarithmic decrement is converging to the value obtained by a linear CFD flutter analysis. The logarithmic decrement is the logarithmic decrease of the amplitude and in this work measured over two consecutive periods. With the linear force evaluation as in Eq. (14) the aerodynamicaly unstable case (IBPA $= +72^\circ$) would exhibit a logarithmic decrement of approx. -2% instead of -3.3%. This shows that the geometric variation term can contribute significantly to the aerodynamic damping und must be accounted for if modal dynamics are used for the CSM solver.

A limit cycle oscillation is simulated with the unstable

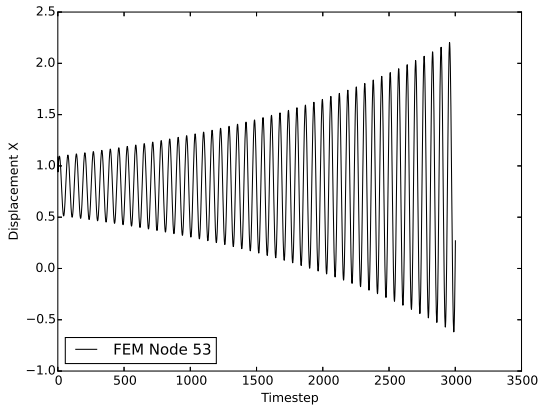

FIGURE 6: Transient x-displacement in the shroud of the excitet mode (IBPA $= +72^\circ$).

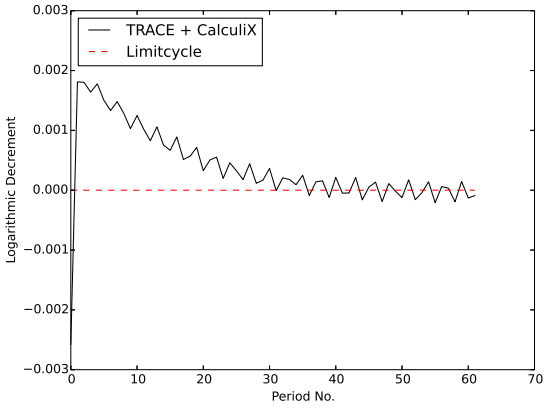

FIGURE 7: Transient logarithmic decrement with conservative surface pressure interpolation.

traveling wave mode (IBPA $= +72^\circ$) and contact dissipation due to dry friction in the joints of the shroud. Figure 9 shows the location of the contact region. Within a small area of the contact region sliding boundary conditions are applied to 6 nodes on each side for the modal analysis in the preprocess. The nonlinear force element and the spring element for contact friction modeling are placed between two adjacent nodes (each belonging to one of the two contact surfaces). Figure 12 shows the convergence of the logarithmic decrement of a coupled simulation with nonlinear contact model. Due to the discrete form of the vibration signal the logarithmic decrement is jagged because the sensitivity with respect to small variations in the signal peaks is high. The nonlinear dissipation in the contact region leads to a limit cycle oscillation of the vibrating system which is reached after approx. 40 periods.

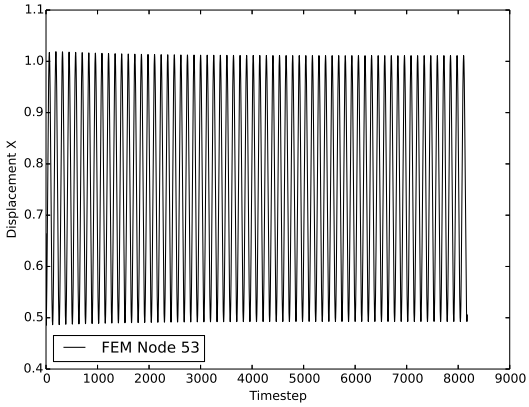

FIGURE 8: Transient displacement with conservative surface pressure interpolation.

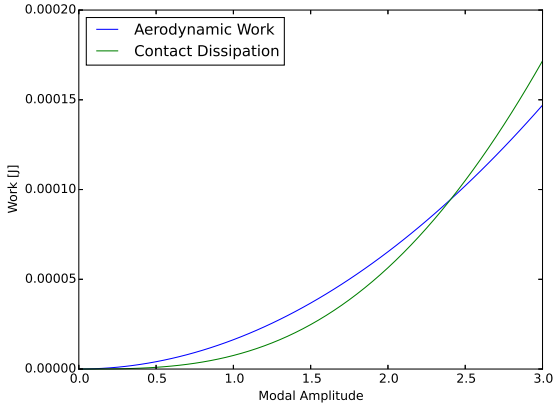

FIGURE 10: Work performed during one vibration period.

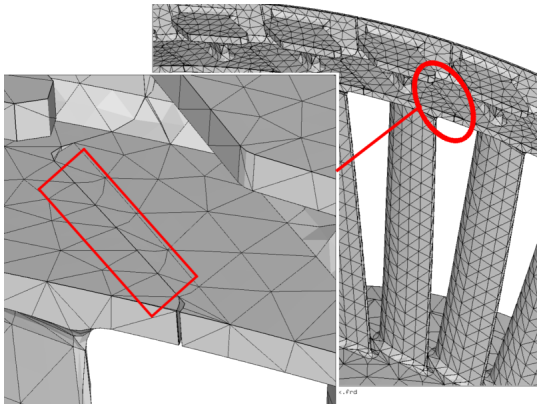

FIGURE 9: Joint location in the shroud of the LPT.

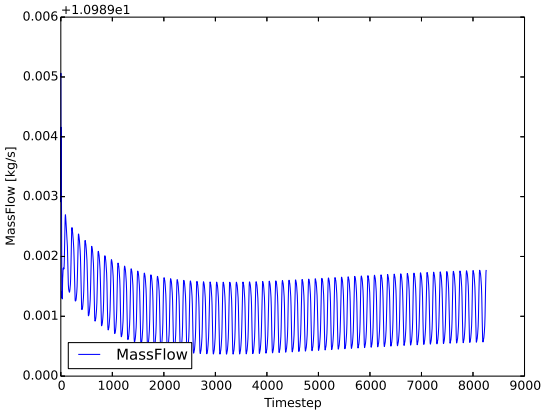

FIGURE 11: Massflow over time.

The initial amplitude (x-displacement amplitude of 0.265 mm in the contact surface) is already very close to the limit cycle amplitude (0.2592 mm) shown in Figure 8. The expected limit cycle amplitude was approximated in advance with a semi analytic evaluation of the contact dissipation and the aerodynamic work performed during one period as a function of the vibrational amplitude (see Figure 10). Therefore the dissipation as a function of vibrational amplitude is determined with numerical integration and the flow response is assumed to be linear resulting in a quadric behavior for the aerodynamic work as a function of amplitude. Furthermore this analysis revealed that only a single stable limit cycle solution exists. The crossing of the work and disspiation graphs at a modal amplitude of 2.406 predicts the stable limit cycle oscillation and corresponds to an x-displacement amplitude of 0.2591 mm in the shroud. It should be mentioned that for modal amplitudes > 3.0 the contact dissipation will continue to increase linearly for the limiting case since the regularized contact friction model will converge to a constant force value for increasing relative velocities. Thus there is a second point for which the contact disspiation and aerodynamic work are equal but which is not a stable LCO solution.

The transient massflow is presented in Figure 11. It oscillates with a very small amplitude and the periodic mean value is slowly converging. Thus the point of operation is slowly changing during the transient simulation. The simulation takes 41 hours on 24 CPUs with 128 timesteps per period. The nonlinear force due to the contact friction is calculated explicitly at each timestep.

In Figure 12 the transient logarithmic decrement of the same simulation as above but with nearest neighbour interpolation for the surface pressure is shown. It can be observed that the oscillation of the blades is not converging to a limit cycle but that the logarithmic decrement becomes negative and the

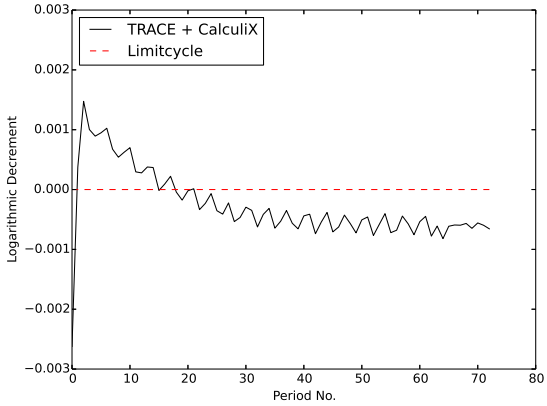

FIGURE 12: Transient logarithmic decrement with nearest neighbour surface pressure interpolation.

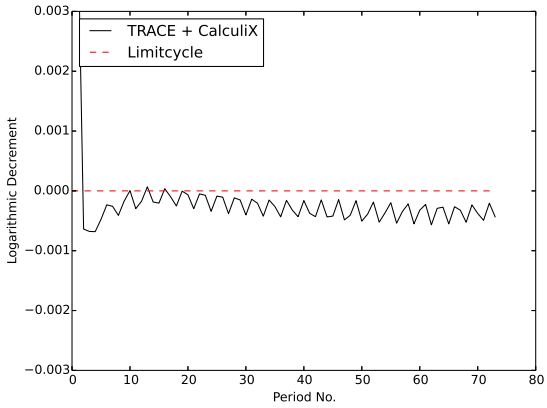

FIGURE 13: Transient logarithmic decrement with conservative surface pressure interpolation and a slightly decreased initial amplitude.

vibration amplitude starts to increase.

A simulation with a slightly decreased initial amplitude (0.219 mm) is shown in Figures 14 and 13. After a long simulation time the vibrational amplitude is 0.221 mm which shows that much more simulation time would be required to come close to the LCO solution.

DISCUSSION AND CONCLUSIONS

In a first step the coupled FSI solver was verified with linear flutter results. The agreement is good and the tendency of coupled vibrational frequency prediction is reasonably good. For the excited or damped vibration the impact of the surface interpolation method does not play a crucial role in the presented testcase. The consistent results are obtained with the

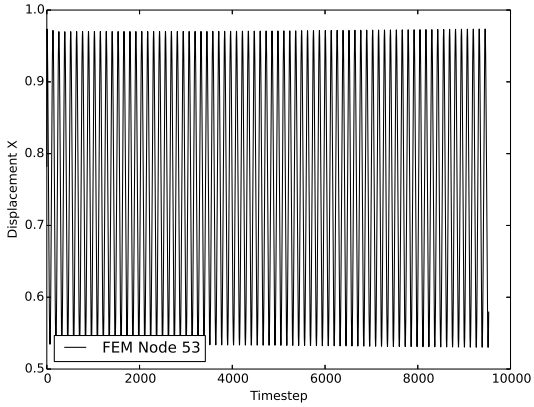

FIGURE 14: Transient displacement with conservative surface pressure interpolation and a slightly decreased initial amplitude.

modal force evaluation according to Eq. (12).

For a limit cycle oscillation the solver is validated against a semi-analytical solution of the balance between aerodynamic work and dissipation due to the nonlinear friction in the joints and the results agree well. The fact that the semi-analytical results agree well shows that the flow response behaves very linear with respect to the vibration amplitude. Only a reasonable simulation time until convergence can be achieved if some information about the LCO solution is available. It is concluded that a time accurate tool is preferably used together with other less expensive methods as a validation or correction tool. The convergence of the mass flow shows, that during the coupled simulation the point of operation of the engine changes slightly. Consequently it must be expected that the results and costs of a time accurate FSI simulation can vary significantly with the type of fluid boundary and initial conditions. The choice of the interpolation method also influences the coupled FSI solver. Good behavior could only be achieved with conservative interpolation for this testcase. If a full FEM model is to be used for time integration then one should use an improved conservative interpolation method. Another possibility would be to use a higher order consistent surface interpolation method (e.g. with radial basis functions) and make sure that the structural mesh is fine enough at the FSI interface.

The results show that the proposed approach of a coupled FSI simulation is useful to carry out a vibration analysis of a fluid-structure system. With a specific number of resolved flow passages in the CFD setup specific families of IBPAs can be analysed seperately with an approporiate artificial force perturbation for initializing the motion of the structure. However not all traveling wave modes can be analysed seperately since for some IBPAs it is required to resolve the full bladerow which in turn leads to all traveling wave modes being resolved. If modal

dynamics for the structural solver are used this can be overcome since in this case selected structural eigenmodes can be artificially damped or excluded from the simulation. The use of phase-lag boundary conditions for the flow solver to simulate a single flow passage is not recommended because phase-lag methods in general require the exact frequency of the perturbations which in case of a coupled flutter simulation is a part of the solution. An approximate frequency for periodic phase-lag boundaries can lead to damped oscillations instead of a (physical) LCO solution [15].

Due to the expensive computational costs more efficient coupled simulation methods are desired. Currently effort is invested in nonlinear frequency domain methods in order to couple solid and fluid Harmonic Balance solvers with each other to develop an efficient analysis technique for LCOs (see e.g. [15]). The presented time accurate method will be used to validate newly developed frequency domain methods and to assess the stability of LCOs.

ACKNOWLEDGMENT

This research was funded by the Deutsche Forschungsgemeinschaft (DFG, German Research Foundation) under grant no. 382141955 and by the Forschungsvereinigung Verbrennungskraftmaschinen e.V. (FVV, Research Association for Combustion Engines eV) under grant no. 6001308. This is gratefully acknowledged.

REFERENCES

[1] Ashcroft, G., Frey, C., and Kersken, H.-P., 2014. "On the development of a harmonic balance method for aeroelastic analysis". In 6th European Conference on Computational Fluid Dynamics (ECFD VI).

[2] Kersken, H.-P., Frey, C., Voigt, C., and Ashcroft, G., 2012. "Time-linearized and time-accurate 3D RANS methods for aeroelastic analysis in turbomachinery". *J. Turbomach.,* ***134***(5), p. 051024.

[3] Krack, M., Salles, L., and Thouverez, F., 2017. "Vibration prediction of bladed disks coupled by friction joints". *Archives of Computational Methods in Engineering,* ***24***(3), pp. 589–636.

[4] Hall, K. C., Thomas, J. P., and Clark, W. S., 2002. "Computation of unsteady nonlinear flows in cascades using a harmonic balance technique". *AIAA J.,* ***40***(5), May, pp. 879–886.

[5] Spiker, M. A., Kielb, R. E., Hall, K. C., and Thomas, J. P., 2008. "Efficient design method for non-synchronous vibrations using enforced motion". No. 43154, pp. 735–747.

[6] Becker, K., Heitkamp, K., and Kügeler, E., 2010. "Recent progress in a hybrid-grid cfd solver for turbomachinery flows". In Proceedings Fifth European Conference on Computational Fluid Dynamics ECCOMAS CFD 2010.

[7] Dhondt, G., 2004. *The finite element method for three-dimensional thermomechanical applications*. John Wiley & Sons.

[8] de Boer, A., van Zuijlen, A. H., and Bijl, H., 2008. "Comparison of conservative and consistent approaches for the coupling of non-matching meshes". *Computer Methods in Applied Mechanics and Engineering,* ***197***(49-50), pp. 4284–4297.

[9] Wendland, H., 2006. "Spatial coupling in aeroelasticity by meshless kernel-based methods". *Oñate, E.(Hrsg.)*.

[10] Wilcox, D. C., 1988. "Reassessment of the scale-determining equation for advanced turbulence models". *AIAA J.,* ***26***(11), Nov., pp. 1299–1310.

[11] van Zuijlen, A. H., 2006. "Fluid-structure interaction simulations: efficient higher order time integration of partitioned systems".

[12] Kersken, H.-P., Ashcroft, G., Frey, C., Wolfrum, N., and Korte, D., 2014. "Nonreflecting boundary conditions for aeroelastic analysis in time and frequency domain 3D RANS solvers". In Proceedings of ASME Turbo Expo 2014.

[13] Uyttersprot, L.", 2014.". PhD thesis, Ph. D. thesis, Delft University of Technology.

[14] Srinivas, K., and Fletcher, C. A. J., 1992. *Computational techniques for fluid dynamics: a solutions manual*. Springer.

[15] Berthold, C. R., 2016. "Development of a coupled fluid-structure simulation method in the frequency domain". Master's thesis, Faculty of Mechanical, Maritime and Materials Engineering (3mE), Delft University of Technology. P&E report number: 2760.

